Electronic Supplementary Material (ESI) for Physical Chemistry Chemical Physics.

Supplementary Information

HSO_3Cl: A Prototype Molecule for Studying OH-stretching Overtone Induced Photodissociation

Juvenal Yosa Reyes[1,2,#], Sebastian Brickel [1,#], Oliver Unke[1], Tibor Nagy[1,3], Markus Meuwly[1,*]

[1]Department of Chemistry, University of Basel, Klingelbergstrasse 80, Basel, Switzerland

[2]Industrial and Systems Engineering Department, National University Bogotá, Carrera 45 # 26-85, Bogotá, Colombia

[3]IMEC, RCNS, Hungarian Academy of Sciences, Magyar tudósok körútja 2., Budapest, Hungary

[#]These authors contributed equally to this work

(Dated: January 18, 2016)

Abstract

Initial parameters for bonds (S=O, S−O and O−H), angles (O=S=O, O−S=O and S−O−H), dihedral (O=S−O−H) and Urey-Bradley (O=S=O, O−S=O and S−O−H) for HSO_3Cl were obtained from previous studies on H_2SO_4.[1]

MS-ARMD employs generalized-exponent Lennard-Jones potentials (or Mie potentials)[2] which are used for HSO_3Cl, between 1-4 (H−Cl and H−O_B or O_C) neighboring atoms.[3] Point charges were obtained by fitting the molecular electrostatic potential (ESP) using the CHELPG scheme within Gaussian09.[4] Initial values for all other parameters were taken or calculated (i.e. for generalized Lennard-Jones) from SWISSPARAM.[5]

Starting with these initial parameters, representative geometries were collected for each molecule (HSO_3Cl, HCl and SO_3) from MD simulations, which cover the regions of the multidimensional PES relevant to the equilibrium dynamics (in total of 4346). A MD simulation was started from the optimized geometry, heated to 300 K, and subsequently equilibrated for 40 ps, followed by 10 ns of free dynamics at constant total energy. To cover the regions of the phase space where the dynamics are sampled after excitation, the above protocol was followed after heating up to 1000 K. Starting along the three trajectories, approximately 1000, 1004 and 2041 (1000 at 300 K and 1041 at 1000 K) geometries were selected for HCl, SO_3 and HSO_3Cl, respectively. Additionally, a rigid scan along the dihedral angles Cl-S-O_A-H in HSO_3Cl was performed resulting in an extra 36 reference data points.

For every representative structure a single point energy was computed at the MP2/6-311G+(2d,2p) level. The energies and structures were subsequently used in a fitting procedure to a functional form:

$$\begin{aligned} V(\mathbf{x}) = & \sum_{\text{bonds}} D_e(1-e^{-\beta(r-r_0)})^2 + \sum_{\text{angles}} K_\theta(\theta-\theta_0)^2 \\ & + \sum_{\text{Urey-Bradley}} K_{\text{UB}}(S-S_0)^2 \sum_{\text{dihedral}} H_\phi(1+\cos(n\phi-\delta)) \\ & + \sum_{\text{impropers}} K_\omega(\omega-\omega_0)^2 \\ & + \sum_{ij} \left\{ \frac{n\varepsilon_{ij}}{m-n} \left[\left(\frac{r_{\min,ij}}{r_{ij}} \right)^m - \frac{m}{n} \left(\frac{r_{\min,ij}}{r_{ij}} \right)^n \right] + \frac{q_i q_j}{4\pi\varepsilon_0 r_{ij}} \right\} \end{aligned} \tag{1}$$

in order to optimize the FF parameters. For this purpose, a downhill SIMPLEX algorithm[6] was

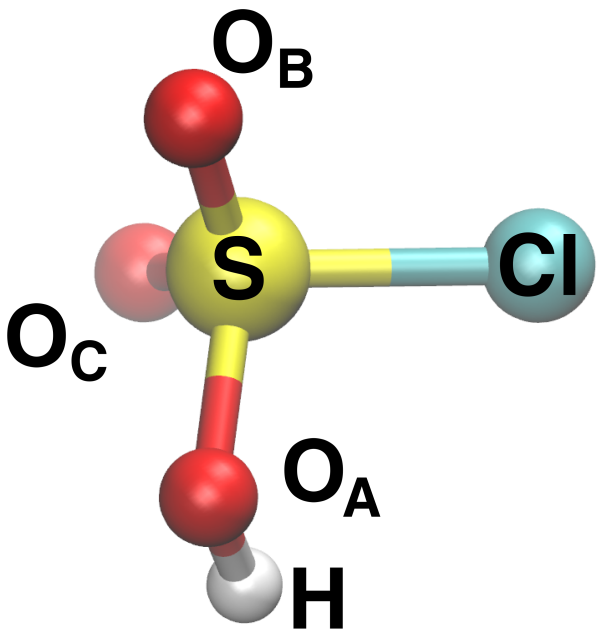

FIG. S-I: Structure of HSO_3Cl with labels.

used.

Similar to H_2SO_4, HSO_3Cl can follow two different pathways: intramolecular H-transfer and HCl elimination ($HSO_3Cl \rightarrow HCl + SO_3$), see Figure 1 in the manuscript.[1,7,8]

With the refined FF parameters for HCl and SO_3, the generalized Lennard-Jones (GLJ) parameters and atomic charges (last term in Eq. 1) were fitted in order to describe the intermolecular interactions for the $HCl\cdots SO_3$ van der Waals complex. Initial values for the GLJ parameters are obtained from the Lennard-Jones parameters between pairs of atoms i and j using the Lorentz-Berthelot combination rules in which ε_{ij} is the geometric mean of ε_i and ε_j and $r_{\mathrm{min},ij}$ is the arithmetic mean of $r_{\mathrm{min},i}$ and $r_{\mathrm{min},j}$. For the GLJ potential, ε_{ij} (> 0) and $r_{\mathrm{min},ij}$ are also the well-depth and the corresponding separation at this energy minimum, respectively.

With this initial parameter set, a new MD simulation for HSO_3Cl was run at 250 K to avoid dissociation. Another 1000 structures were collected and single point energies were computed at the MP2 level and included in the fit. The total number of structures that were used for the final fitting was 3376.

Following the same protocol as for H_2SO_4[1,3], surfaces for the reactant (HSO_3Cl) and products ($HCl + SO_3$) need to be combined and a permutation invariant force fields for the different, but chemically equivalent, product channels are needed for the global surface. In total three different surfaces characterize the intramolecular H-transfer states and one surface is used for HCl elimination. In MS-ARMD the FFs for the individual states i (connectivities) are mixed according to

$$\sum_{i=1}^{n} w_i(\vec{x}) V_i(\vec{x}) \tag{2}$$

where $w_i(\vec{x})$ are normalized weights of the raw weights $w_{i,0} = \exp\Big(- \big(V_j(\vec{x}) - V_{min}(\vec{x})\big)/\Delta V \Big)$, depending on the i-th PES $V_i(x)$. However, simple mixing will lead to discontinuous behavior in the barrier region[3] and typically overestimate the barrier, see features ($*$) in Figure S-II (lower panel). In order to address this point, Gaussian $\times$ polynomial functions (GAPOs) are used. Reference data in the barrier region and along the minimum energy paths (MEPs) were determined from quadratic synchronous transit (QST2) calculations at the MP2/6-311G+(2d,2p) level and the GAPOs were fitted to them while freezing the remaining FF terms at their previously optimised values. More detailed information about the GAPO function can be found in Nagy et al.[3] The barrier height of the intramolecular H-transfer is fitted with three GAPOs, each one with a polynomial of order four, leading to a symmetric intramolecular MEP. HCl elimination is represented with three GAPOs, each one with a polynomial of order five.

A comparison between the MP2 reference energies and the FF with and without GAPOs is provided in Figure S-II. Figure S-II (lower panel) shows the potential energy difference between the FF with and without the corrected GAPOs function. The main difference is shown in those zones where the two IRCs are located. Deviations less than 0.16 kcal/mol are found for the structures collected after excitation with $\nu_{OH} = 6$ (see Figure S-II), while for the thermal equilibrium at 300 K the effect of the GAPO functions is negligible. In that way one is sure that the correction functions only affects the energy of those structures close to the transition state.

Table S-I compares the geometric parameters for the equilibrated structures of the three molecules, obtained with MP2 and the FF. For the two photofragments there are no deviations between the *ab initio* and the FF bond lengths and angles. For HSO_3Cl slight but insignificant deviations were

found for bond length, angles, and dihedrals. Overall, the structures are well reproduced.

Table S-II shows the computed vibrational frequencies for HSO_3Cl and SO_3. All MP2 frequencies were scaled with a factor of 0.97 (MP2/6-31+G(d,p)[9] and MP2-fc/6-311G(d,p)[10]). As the FF is based on MP2 calculations, the vibrational frequencies from the normal mode analysis using the FF were also scaled with the same scaling factor. Comparison between the two sets of values shows a non-systematic difference between the MP2 and the FF energies. These differences are small for both molecules. When comparing the values obtained with MP2 and FF with experimental values it was found that the MP2 is somewhat closer to the measured values than the FF.

Final State Analysis: For the final state analysis, the total energy of the system was decomposed into translational (E_{trans}), rotational (E_{rot}), and vibrational (E_{vib}) components of each fragment. The translational energy is $E_{\text{trans}} = \frac{1}{2}Mv_{\text{CM}}^2$ where M and v_{CM} denote the mass and the velocity of the center of mass for each fragment (SO_3 and HCl). Following classical mechanics, the angular momentum vector of a reaction product (with N atoms) is $\mathbf{L} = \sum_{i=1}^{N} m_i \left(\mathbf{r}_i - \mathbf{r}_{\text{CM}}\right) \times \left(\mathbf{v}_i - \mathbf{v}_{\text{CM}}\right)$. Here, $\mathbf{r}_{\text{CM}}$ and $\mathbf{v}_{\text{CM}}$ denote the position and the velocity vectors of the center of mass for each fragment. This yields the rotational energy $E_{\text{rot}} = \frac{1}{2}\mathbf{L}^{\text{T}}\Theta^{-1}\mathbf{L}$ where $\Theta = \sum_{i=1}^{N} m_i \left(\mathbf{E}r_i^2 - \mathbf{r}_i\mathbf{r}_i^{\text{T}}\right)$ is the moment of inertia tensor of the fragment and $\mathbf{E}$ is the unit matrix. HCl as a linear molecule can only rotate around axes through its center of mass which are orthogonal to the HCl bond.

The angular momentum quantum number j is calculated from the classical-quantum correspondence relationship $L^2 = j(j+1)\hbar^2$ in which $\hbar$ is Planck's constant. The orbital angular momentum ($\mathbf{L}_{\text{orbital}}$) can be determined from the individual angular momenta of the fragments and from the conservation of total angular momentum.

From E_{trans} and E_{rot} the vibrational energy of each product is determined through the relationship $E_{\text{tot}} = E_{\text{pot}} + E_{\text{kin}}$. Utilising that E_{vib} is a part of E_{kin}, relative to the center of mass with addition of the intramolecular potential energy of the given reaction product, the vibrational energy can be expressed as $E_{\text{vib}} = E_{\text{kin}} - E_{\text{trans}} - E_{\text{rot}} + V$. Once the two fragments have moved sufficiently far from the interaction region (here taken as 20 Å between the SO_3-sulfur and the HCl-chlorine), the translational and rovibrational energy of each fragment will be constant. As the vibrational and rotational modes in each fragment keep on exchanging energy if the angular momentum is

nonzero, these quantities are averaged over periods much longer (i.e. 5 ps) than the characteristic time for vibrations within the molecules.

TABLE S-I: Comparison of MP2 and force field geometric parameters for the equilibrium of HSO_3Cl, SO_3 (symmetry D_{3h}, X = A, B, C) and HCl.

	MP2	**Force Field**
	HSO_3Cl	
Bonds (Å)		
S-Cl	2.066	2.074
S-O_B	1.432	1.429
S-O_C	1.424	1.428
S-O_A	1.596	1.602
O_A-H	0.969	0.978
Angles (°)		
O_C-S-O_B	124.5	124.3
O_C-S-O_A	109.1	109.0
O_B-S-O_A	106.3	106.4
Cl-S-O_B	107.4	107.3
Cl-S-O_C	106.6	106.8
Cl-S-O_A	100.3	100.6
S-O_A-H	107.7	108.1
Dihedral (°)		
O_B-S-O_A-H	164.8	164.6
O_C-S-O_A-H	28.2	28.3
Cl-S-O_A-H	-83.6	-83.7

	MP2	**Force Field**
	SO_3	
Bonds (Å)		
S-O_X	1.44	1.44
Angles (°)		
O_X-S-O_Y	120.0	120.0
	HCl	
Bonds (Å)		
Cl-H	1.27	1.27

TABLE S-II: computed and experimental vibrational frequencies for HSO_3Cl and SO_3. MP2 and FF scaled by a factor of 0.97.

MP2 cm^{-1}	**Experimental cm^{-1}**	**FF cm^{-1}**
HSO_3Cl		
252.5		250.7
277.7		306.8
355.7		315.6
385.4		376.6
444.3		493.9
479.3	513.0	507.0
578.4	614.0	538.8
798.3	852.0	799.1
1149.1		1106.8
1170.0	1235.0	1141.0
1411.5	1455.0	1364.5
3663.9	3587.0	3656.5
SO_3		
474.4	498	457.2
509.6 509.8	530	496.7 496.7
1020.6	1065	1080.3
1366.4 1367.3	1391	1363.1 1363.2

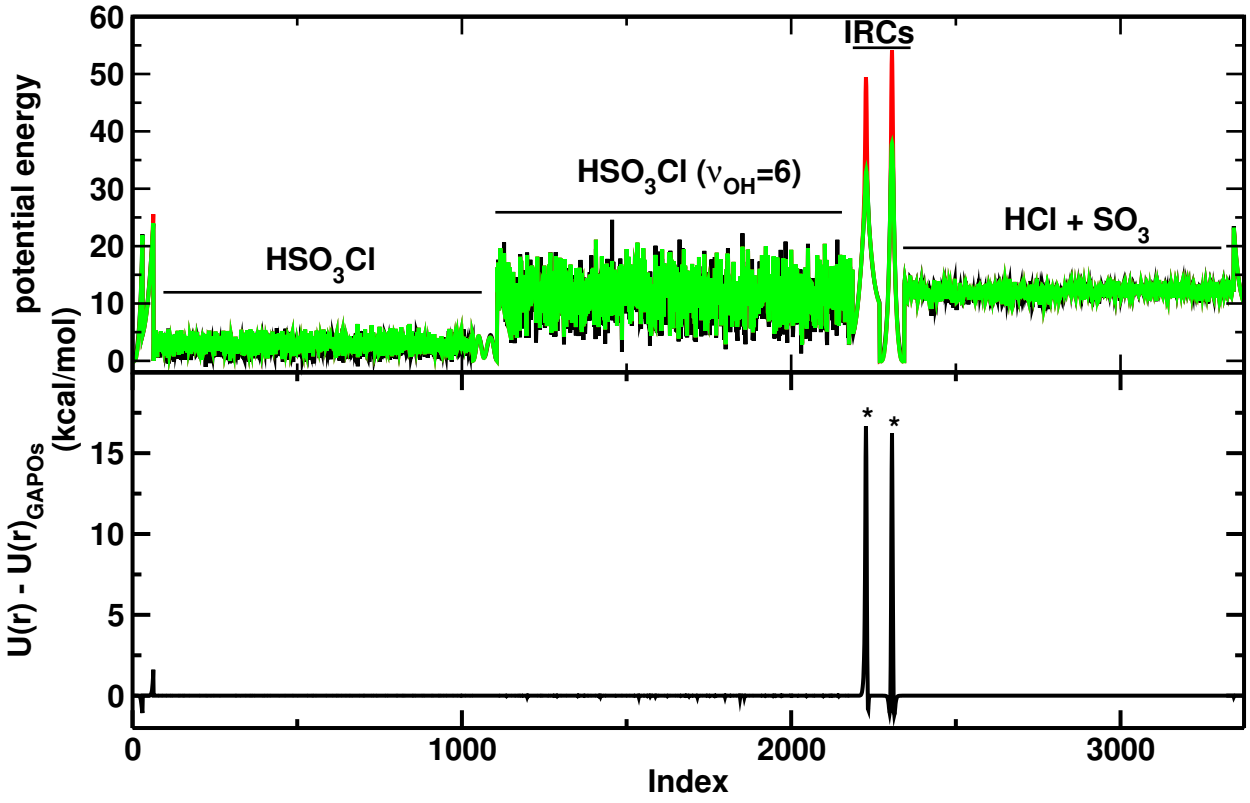

FIG. S-II: Potential energy as a function of the molecule index. Top panel) Comparison between FF with (red) and without GAPOs (green) and MP2 reference points (black). Bottom panel) Potential energy difference between FF with and without GAPOs.

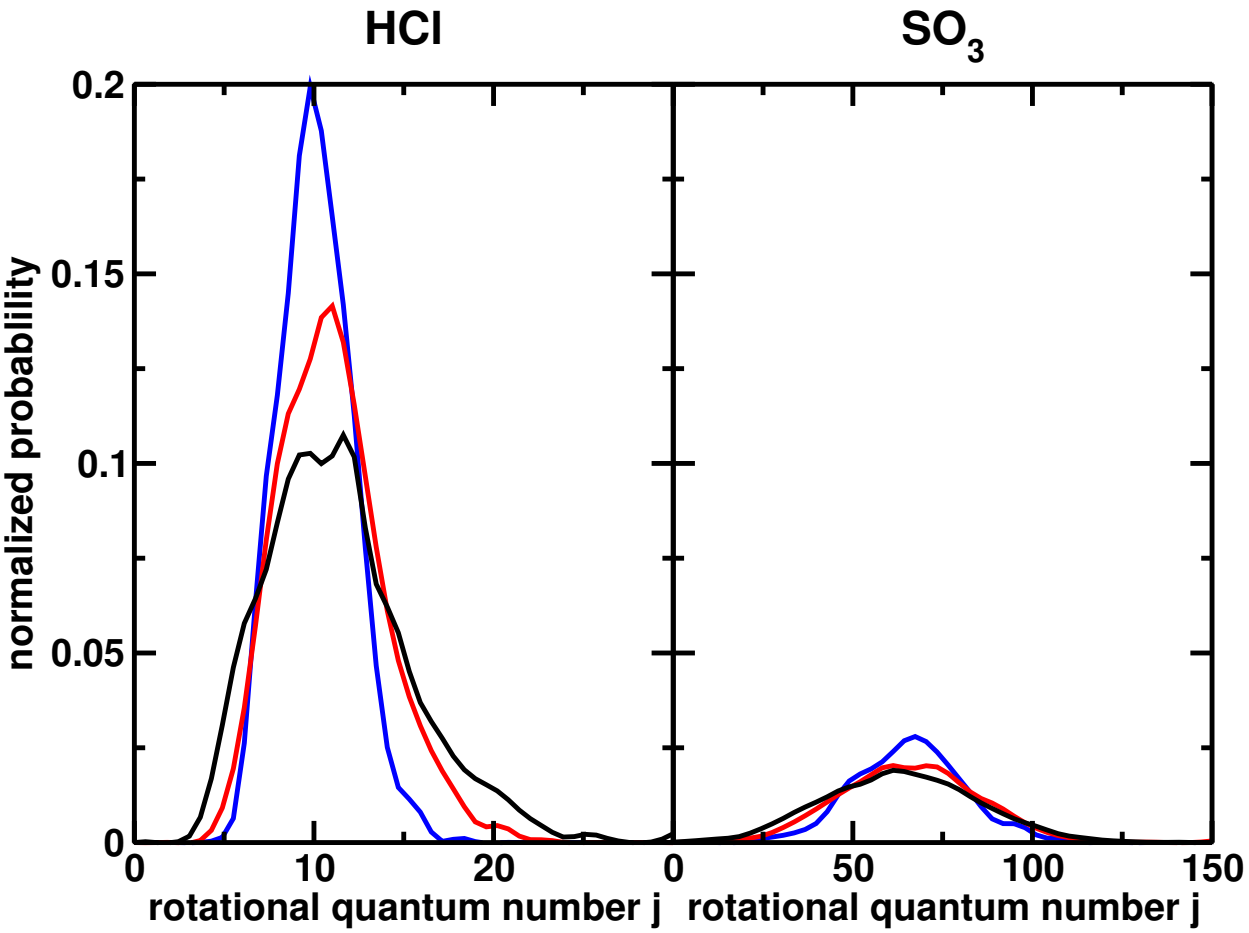

FIG. S-III: Rotational quantum number j distribution for HCl and SO_3 . Blue, red and black represents $\nu_{OH} = 4$, 5 and 6 respectively.

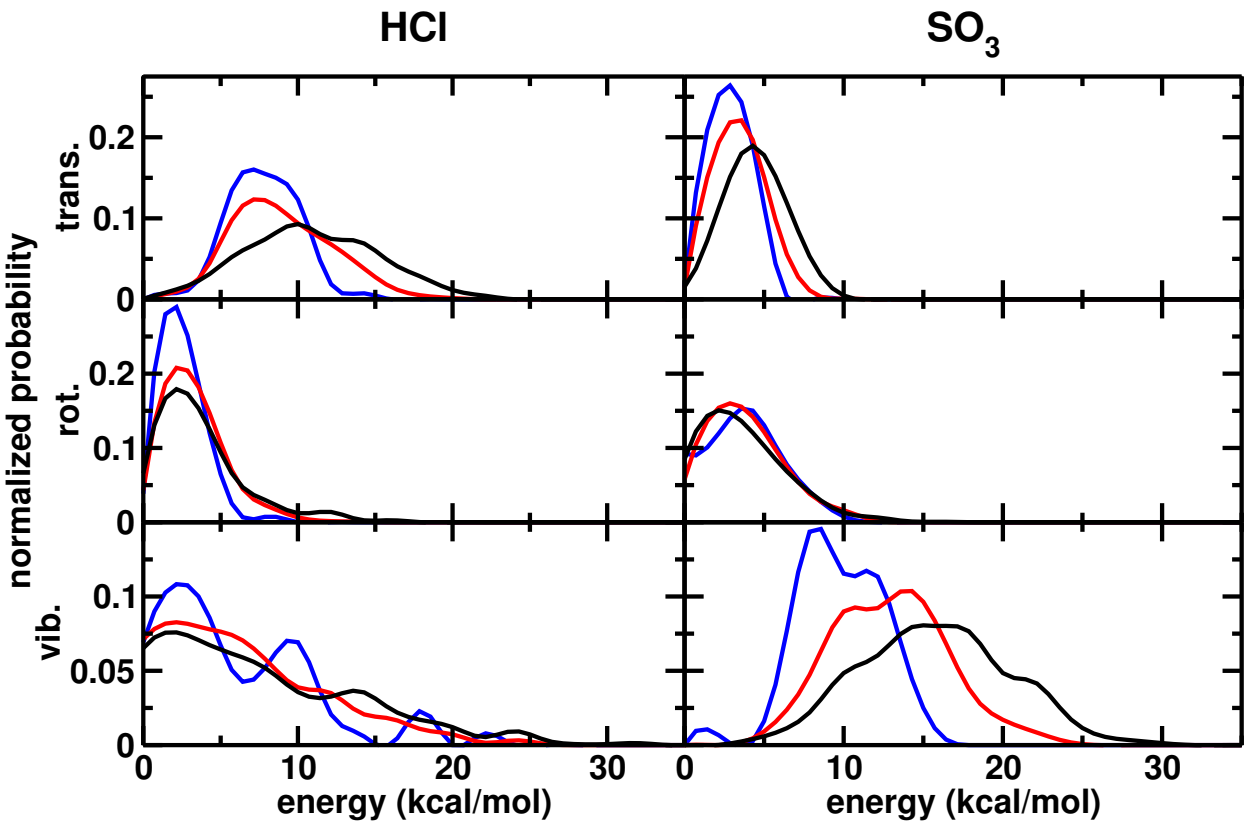

FIG. S-IV: Final state analysis for HCl and SO_3 with initial conditions from the Monte Carlo sampling. Blue, red, and black curves correspond to excitation of $\nu_{OH} = 4$, 5 and 6, respectively. See Figure 5 in the manuscript for the final state analysis from simulations with *NVE* initial conditions.

[1] J. Yosa, T. Nagy and M. Meuwly, Phys. Chem. Chem. Phys., 2014, **16**, 18533 – 18544.

[2] G. Mie, Ann. Phy., 1903, **316**, 657–697.

[3] T. Nagy, J. Yosa and M. Meuwly, J. Chem. Theory. Comput., 2014, **10**, 1366 – 1375.

[4] C. Breneman and K. Wiberg, J. Chem. Comp., 1990, **11**, 361373.

[5] V. Zoete, M. A. Cuendet, A. Grosdidier and O. Michielin, J. Comput. Chem., 2011, **32**, 2359–2368.

[6] J. Nelder and R. Mead, Chem. Phys., 1965, **7**, 308 – 313.

[7] Y. Miller and R. B. Gerber, J. Am. Chem. Soc., 2006, **128**, 9594 – 9595.

[8] P. Gupta, J. R. Lane and H. G. Kjaergaard, Phys. Chem. Chem. Phys., 2010, **12**, 8277–8284.

[9] Y. Zhao, B. J. Lynch and D. G. Truhlar, J. Phys. Chem. A, 2004, **108**, 4786–4791.

[10] A. P. Scott and L. Radom, J. Phys. Chem., 1996, **100**, 16502–16513.